International Journal of Non-Linear Mechanics 118 (2020) 103263

Contents lists available at ScienceDirect

International Journal of Non-Linear Mechanics

journal homepage: www.elsevier.com/locate/nlm

On thermo-viscoelastic experimental characterization and numerical modelling of VHB polymer

Zisheng Liao [a,b], Mokarram Hossain [b,*], Xiaohu Yao [a], Markus Mehnert [c], Paul Steinmann [c,d]

[a] School of Civil Engineering and Transportation, South China University of Technology, 510640 Guangzhou, Guangdong, China
[b] Zienkiewicz Centre for Computational Engineering (ZCCE), College of Engineering, Swansea University, SA1 8EN, United Kingdom
[c] Chair of Applied Mechanics, University of Erlangen–Nuremberg, 5 Egerland Strasse, Erlangen, Germany
[d] Glasgow Computational Engineering Centre (GCEC), University of Glasgow, Glasgow G12 8QQ, United Kingdom

ARTICLE INFO

Keywords:
VHB polymer
Thermo-viscoelasticity
Temperature dependence
Dielectric elastomers

ABSTRACT

Recently, the so-called Very High Bond (VHB in short) tape has proven to be an ideal polymer for producing devices made of electric field-responsive functional materials, e.g., actuators in soft robotics, stretch sensors in wearable devices, and energy harvesters generating power from ambient motions. The VHB polymer is commercially available in several thicknesses. For this study, we have selected VHB 4905 due to its wide use as a common material for dielectric elastomers. The acrylic-based polymer is highly deformable, extremely viscoelastic, and highly sensitive to temperature fluctuations. Hence, in order to understand its mechanical and electro-mechanical behaviour, extensive experiments need to be conducted to unravel temperature dependencies in addition to strain-rate dependences. In this study, we present a wide variety of temperature experiments ranging from -30°C to 80°C at various strain rates and stretch levels under homogeneous deformation and temperature fields. The study demonstrates a pronounced influence of the temperature on the mechanical response of the VHB polymer. For VHB within the temperature range of our study, an increased temperature mechanically softens the material and vice-versa. After conducting a wide range of experiments, we propose a finite strain thermo-viscoelastic constitutive model that is an extension of a phenomenologically-motivated model where a non-linear evolution law is devised based on the classical concept of the multiplicative decomposition of the deformation gradient. Then, decoupled one-dimensional equations are derived and fitted to experimental data to identify relevant material parameters appearing in the model. The thermo-viscoelastic model validation shows its reasonably good capability to predict the experimental results.

1. Introduction

Smart or functional materials undergo a change in size, shape, stiffness, and other mechanical attributes upon the application of external fields (temperature, electric or magnetic field). Recently, among other smart materials, electro-active polymers (EAPs) drew considerable attention due to their wide range of applications. In EAPs, the external field is the electric field resulting from an electric potential difference. In contrast to traditional functional materials (e.g., piezoelectric materials), EAPs can react with extremely large strains up to 400% under a combined electromechanical loading [1–4]. Such large scale actuations make them very promising candidates for use in various engineering applications, for example, as sensors, actuators, and energy harvesters. EAPs in actuators are utilized in the form of a thin film that is sandwiched between two compliant electrodes and then exposed to an electric potential difference, which creates Maxwell forces between the electrodes. In summary, such a process can be considered as a mechanical output as a result of electric stimuli [1–3].

Basically, two major groups of polymers have been used as EAPs, namely acrylic-based polymers (e.g., VHB) and silicon-based polymers. However, due to insufficient electro-mechanical coupling effects, unfilled pure polymers are currently not optimal choices for dielectric applications. In order to enhance actuations, a significant amount of effort has been directed towards developing polymer composites with enhanced actuation properties. In this case, three major techniques have actively been explored, e.g. polymers filled with highly piezoelectric particles, polymer blends of two or more different dielectric polymers, and syntheses of new polymers with tailored actuation characteristics, see Alshammari et al. [5], Dang et al. [6], Ellingford et al. [7], Keip et al. [8], Hossain [9]. Despite such limitations, VHB is being considered as one of the most widely used EAP candidates for

* Corresponding author.
E-mail addresses: l.zisheng@mail.scut.edu.cn (Z. Liao), mokarram.hossain@swansea.ac.uk (M. Hossain), yaoxh@scut.edu.cn (X. Yao), markus.mehnert@fau.de (M. Mehnert), paul.steinmann@fau.de (P. Steinmann).

https://doi.org/10.1016/j.ijnonlinmec.2019.103263
Received 16 May 2019; Received in revised form 28 August 2019; Accepted 3 September 2019
Available online 9 September 2019
0020-7462/

making actuator prototypes due to its moderate actuation properties, large stretchability, low susceptible to dielectric breakdowns, and commercial availability. The VHB series (mainly VHB 4910 and VHB 4905 of 1 mm and 0.5 mm thicknesses, respectively) are very soft materials that exhibit physically non-linear viscoelastic behaviour with a very high stretchability, extreme temperature sensitivity, and pronounced dissipative behaviours, see Wissler and Mazza [10], Hossain et al. [11], Mehnert and Steinmann [12].

Despite a wide range of potential applications of VHB polymer, extensive mechanical and electro-mechanical experimental characterizations at large strains are limited in the literature. In an effort to quantify viscoelastic behaviour of this important polymer, Wissler and Mazza [10] published one of the earliest experimental works. They performed various single-step relaxation and creep experiments at room temperature. For a thorough understanding of VHB's viscoelastic behaviour, a comprehensive mechanical characterization by various experimental tests was performed by Hossain et al. [13]. In contrast to the earlier works of Wissler and Mazza [10], Hossain et al. [13] performed several sets of experiments that are essential in characterizing a viscoelastic material, e.g., single-step relaxation tests, multi-step relaxation tests, monotonic tests, and loading–unloading cyclic tests at different strain rates and at various extent of strains. Since VHB has a high stretchability, Patra and Sahu [14] conducted viscoelastic experiments on VHB 4910 up to a strain of twelve hundred percent. Furthermore, Sahu et al. [15] performed experimental investigations on the same material and found that the material possesses strong time-dependent creep and stress relaxation. It has been shown that the creep and stress relaxation characteristics vary with the holding stress and holding strain, respectively.

Very recently, Mehnert and Steinmann [16] did experiments on VHB 4905 in order to quantify the influence of conductive electrodes on the mechanical stress responses. They found that the influence of a Carbon conductive grease, an essential component of electro-mechanical experiments, on the mechanical stress of VHB 4905 is significant and cannot be neglected. Note that all of the above-mentioned experiments have been conducted assuming a uniaxial type homogeneous deformation discarding the influences of a temperature field. Most of the actuator devices are fabricated by pre-stretching the polymer under a pure shear deformation. Therefore, very recently, a detailed quasi-static study under a pure shear deformation mode was conducted on VHB 4910 polymer by Ahmad and Patra [17], Ahmad et al. [18]. Although viscoelastic experimental studies under a purely mechanical load of either VHB 4910 or VHB 4905 are available now, to the best of the authors' knowledge, there is no extensive experimental work that deals with thermo-viscoelastic characterizations and constitutive modelling of VHB. Note that Guo et al. [19] conducted a few experiments on VHB 4910 to show temperature dependencies on relaxation functions. A complete thermo-viscoelastic characterization that includes standard experimentation, i.e. loading–unloading cyclic tests, single-step and multi-step relaxation tests and quasi-static experiments at very slow strain rates under various temperatures, has not been performed yet. Moreover, obeying the relevant laws of thermodynamics, a constitutive modelling framework needs to be developed in a three-dimensional framework that can easily be implemented in a finite element framework for the simulation of inhomogeneous deformations.

The constitutive modelling and numerical simulation of viscoelastic and thermo-viscoelastic behaviour of polymeric materials at large strains has been an active field of research for several decades. Some classical modelling approaches at finite strains are due to Lion [20], Holzapfel and Simo [21], Holzapfel [22], Simo [23], Kaliske and Rothert [24], Bergstroem and Boyce [25,26], Miehe et al. [27,28], Dal and Kaliske [29], Yuhai et al. [30], Saxena et al. [31]. In most models, the multiplicative decomposition of the deformation gradient is performed into elastic and inelastic parts that yield differential-type viscoelastic formulations, cf. Huber and Tsakmakis [32], Reese and Govindjee [33,34], Amin et al. [35,36], Koprowski et al. [37,38], Johlitz et al. [39,40], Masri et al. [41], Rebouah and Chagnon [42], Haldar and Pal [43]. In this case, the total stress is decomposed into an equilibrium stress, that corresponds to the stress response at an infinitely slow rate of strain or the stress response when the time-dependent viscous effect is completely diminished, and a viscosity-induced overstress. To incorporate temperature influences into a viscoelastic model, most of the earlier works adopt the concept of the so-called Time–Temperature-Superposition Principle (TTS) which is only valid for thermo-rheologically simple materials, see for example [44–46]. For developing thermo-viscoelastic models in a thermodynamically consistent way, Lion [20], Sedlan [47], Reese and Govindjee [34], Behnke et al. [48], Dippel et al. [49], Scheffer et al. [50,51], Johlitz et al. [40], Mehnert et al. [16,52] proposed constitutive frameworks that are based on finite strain evolution laws and are not only valid for thermo-rheologically simple materials but also for generic thermo-viscoelastic polymers.

Similar to the experimental characterization, the constitutive modelling of the viscoelastic behaviour of VHB 4910 is limited. For the modelling of the time-independent response (hyperelasticity) of the extremely stretchable polymer, several phenomenologically-motivated energy functions, e.g., Neo-Hooke, Mooney–Rivlin, Ogden, Yeoh, were used by Wissler and Mazza [10]. To capture the time-dependent behaviour of the polymer, they further extended the model in line with the so-called quasi-linear viscoelasticity. Thermodynamically consistency of the model, an important criterion of material equations for modelling inelasticities, is not proven in this work. After conducting an extensive viscoelastic experimental study, Hossain et al. [13] proposed a thermo-dynamically consistent viscoelastic model which is an extension of the classical Arruda–Boyce model with a finite strain linear evolution law as proposed by Linder and co-workers [53,54]. This model fitted well all relevant viscoelastic data of VHB 4910. Patra and Sahu [14] proposed a visco-hyperelastic model for capturing the time-dependent behaviour of VHB 4910 where they used a two-parameter Gent model for the hyperelastic part and an integral-type memory function for the time-dependent contribution. Their model also fitted well all relevant data up to a strain of twelve hundred percent.

The aims of the current contribution are twofold. On the one hand, a complete thermo-viscoelastic mechanical characterization of VHB 4905 is presented considering some standard experiments suitable for viscoelastic polymers at large strains, e.g. loading–unloading cyclic tests, quasi-static tests at very slow strain rates, single-step relaxation tests, and multi-step relaxation tests under homogeneous thermo-mechanical loads. On the other hand, a thermodynamically consistent phenomenologically-motivated geometrically non-linear thermo-viscoelastic material model is developed for the VHB polymer. At this stage, all experiments are performed under homogeneous deformation, for both mechanical and thermal loads. Hence, the three-dimensional thermo-viscoelastic model is decoupled to a set of one-dimensional differential equations. After that, all relevant parameters appearing in the model are identified by a simultaneous optimization routine. Once all necessary material parameters are identified, the results are validated with the data that are not included during the identification process.

The paper is organized as follows: in Section 2, a brief description is presented outlining the experimental set-up, which is utilized to perform the experiments in our laboratory. In addition to the description of the experimental procedures, experimental results are also analysed in this section. After that, an overview of the finite strain thermo-mechanics of polymeric materials is depicted in Section 3. Furthermore, a specified constitutive model for the finite strain thermo-viscoelasticity of polymeric materials is presented in Section 3.2 while in the same section, the constitutive equations are formulated in a one-dimensional form suitable for the parameter identification as well as for the simulation and model validation. In Section 4, the simulation and validation of the model with the experimental data are demonstrated and discussed. Finally, concluding remarks close the paper.

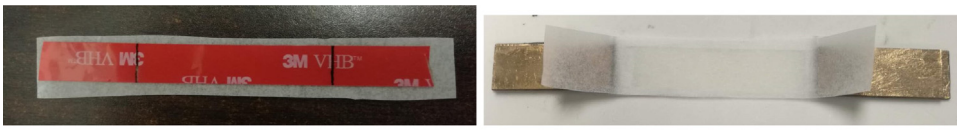

Fig. 1. Specimen preparation. (a) Step 1: VHB tape with a required length is attached to a clean silicon paper, (b) Step 2: after removal of the red protective surface of VHB. (For interpretation of the references to colour in this figure legend, the reader is referred to the web version of this article.)

Fig. 2. A complete thermo-viscoelastic testing system: (1) is the main framework of the Instron 5567, (2) is the control computer, (3) is the temperature chamber, (4) is the force transducer to monitor the applied force, and (5) is the crosshead of (1).

2. Thermo-viscoelastic experimental study

Extensive and systematic experimental characterizations are carried out on the acrylic-type VHB 4905 polymer by a universal material test machine (Instron 5561). To accurately quantify the viscoelastic behaviour of a polymeric material, quasi-static tests at very slow strain rates, loading–unloading cyclic tests, single-step and multi-step relaxation tests at various strain levels, strain rates and temperatures are essential, see Lion [20], Johlitz et al. [39,40], Hossain et al. [13], Mehnert and Steinmann [12], Amin et al. [35,36], Koprowski et al. [37,38], Dippel et al. [49], Scheffer et al. [50,51], Xiang et al. [30]. Hence, in the following sections, the experimental procedures and related results covering the above mentioned four major characterization techniques will be discussed in detail.

2.1. Specimen preparation

For the thermo-viscoelastic experimental characterization outlined in this paper, among other brands, we have chosen the acrylic VHB 4905 polymer[1] produced by 3M^{TM}. The commercially available tape has a thickness of 0.5 mm. For this study, we have purchased a 10 mm wide roll-like tape that was obtained from 3M. Note that 0.5 mm thick VHB polymer is selected for this study as it will be comparatively easier to maintain homogeneous temperatures during experiments along the thickness direction. For the tests at room temperature (20 °C), specimens with a length of 100 mm and a width of 10 mm are selected, maintaining a 10:1 ratio, ideal for a uniaxial homogeneous deformation mode, see Wissler and Mazza [10], Hossain et al. [13], Liao et al. [44], Patra and Sahu [14]. However, due to the displacement limit of the universal test machine inside the temperature chamber, we had to use shorter specimens, i.e. a length of 20 mm which is used only for a few temperature tests. Hence, tensile stresses of different length specimens (100 mm, 50 mm and 20 mm) at the same conditions (same deformation, same strain rates, and same temperatures) are compared to each other. The results coincide with each other which means that the shorter specimen length (20 mm) does not influence the homogeneous stress field along the specimen length.

VHB 4905 is a very soft double-sided bonding tape that is difficult to handle. Therefore, prior to each test, a careful and meticulous preparation technique is necessary to ensure that the specimen is not disturbed or deformed significantly from its original undeformed condition where any pre-deformation due to disturbances might affect the accuracy of the test results. Due to its sticky property, VHB 4905 is widely used as an adhesive tape for many industrial and household applications. Hence, to deal with its stickiness, we use clean silicon paper to cover both sides of the tape before sample preparations. The clean and smooth silicon paper is adhesion free so that it could be peeled off easily from the specimen when the test is about to begin. The whole preparation process is as follows. In Step 1 (cf. Fig. 1a), we attach the tape to the surface of a silicon paper with a required length such as 90 mm (i.e., a 50 mm gauge section and a 20 mm gripping section). Then a black marker is used to identify the gauge section with the help of a ruler and a calliper as is shown in Fig. 1(a). In Step 2 (cf. Fig. 1b), the red protective thin film of both ends is peeled off until the marked lines. For large strain tests, the specimen could possibly slide out from the copper shim. Therefore, another layer of the same VHB 4905 is taped between the shim and the specimen. With this extra layer of tape with sticky characteristics, sliding out can effectively be reduced. Finally, we peel off the entire protective film in the gauge section carefully, and then put another silicon paper over the specimen to protect it from any dust, as is shown in Fig. 1(b). The shims make the specimen easy to be clamped in the grippers and ensure a correct length of the gauge section of the specimen.

2.2. Experimental set-up

The universal test machine Instron 5567 is placed in a customized temperature chamber as shown in Fig. 2, where (1) is the main framework of the Instron 5567, (2) is the control computer, (3) is the temperature chamber, (4) is the force transducer to monitor the applied force, and (5) is the crosshead of (1). A force sensor of ±50 N maximum capacity is used which has a precision of 0.001 N. The chamber can regulate the temperature from −50 °C to 150 °C. At room temperature, i.e., without the use of the temperature chamber, the displacement limit of the machine is 800 mm, while within the chamber, the limit is confined to 200 mm. The maximum loading speed of the crosshead is

[1] https://www.3m.com/3M/en_US/company-us/all-3m-products/~/3M-VHB-Tape-4905.

(a) (b)

Fig. 3. (a) Temperature monitor device, (b) tensile test preparation equipment.

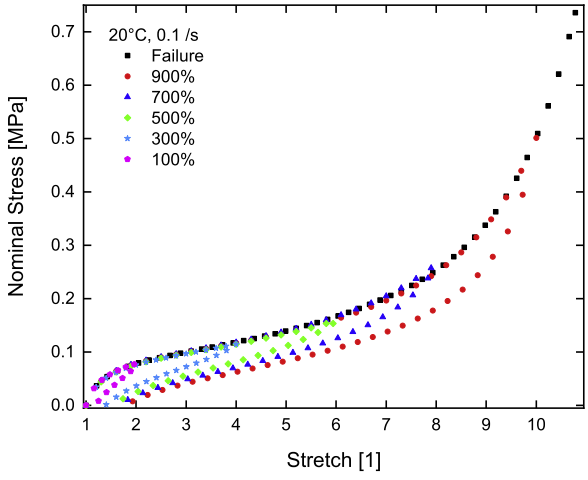

Fig. 4. Stretchability of VHB 4905 polymer at the reference temperature (20 °C). In this study, the material fails at $\lambda = 11$ with a stretch rate of 0.1/s.

8 mm/s. The test machine interacts with the control computer via the Bluehill® universal user interface software.

All results presented in this paper are expressed as the Piola (nominal) stress (i.e., applied force divided by the initial undeformed cross-sectional area) against the corresponding stretch. Strain rates are the time derivative of the engineering strain (i.e., applied displacement divided by the initial length of the gauge section). At least two hundred data points of each test are acquired, and a smoothing technique is applied to the results to reduce noise. To ensure reproducibility of all results, each experiment is repeated three times and the average is taken as a representative result. Prior to an experiment, a de-humidifier is used to control the humidity of the room environment. Besides, an air conditioner is used to control the room temperature at 20 °C. For tests needed to be regulated at a target temperature, specimens are conditioned for fifteen minutes to achieve a stable temperature, which can be monitored through an in-built temperature sensor, as is shown in Fig. 3(a). A fifteen minutes period is sufficient for the temperatures of our thin specimens (0.5 mm) to be homogeneous across the thickness direction. After these procedures of specimen preparation, we mount the specimen on the upper and lower grippers, peel off the silicon paper gently without any pre-tension, regulate the temperature if necessary, and start the test, as is shown in Fig. 3(b).

2.3. Loading-unloading cyclic experiments

In order to characterize the viscoelastic behaviour of the VHB polymer, at first cyclic experiments are carried out applying different deformations, strain rates, and temperatures. In these experiments, we adopt three different strain levels, i.e., 100%, 200%, and 300%, three different strain rates, i.e., 0.1/s, 0.05/s and 0.03/s, and nine different temperatures, i.e. 80 °C, 60 °C, 40 °C, 20 °C, 10 °C, 0 °C, −10 °C, −20 °C, and −30 °C. Note that according to the VHB performance manual supplied by 3M, the acrylic-based polymer goes through its glass transition temperature (T_g) at approximately −40 °C. Results are presented in Figs. 5–8. In Fig. 5, strain-dependent results are presented ranging from −20 °C to + 60 °C temperatures while experiments are conducted at a strain rate of 0.1/s with strains of 100%, 200%, and 300%. These graphs indicate that at all tested temperatures, a larger strain results in a bigger hysteresis with a larger residual strain. Moreover, it is clear that the nonlinearity of the stress–stretch response is getting stronger from a higher to a lower temperature at the same strain. These results also demonstrate that the VHB 4905 becomes less dissipative with an increasing positive temperature.

From Fig. 7, it can clearly be seen that at a fixed strain rate (i.e., 0.1/s) and deformation (i.e., 200%), a decreasing temperature not only results in increasing hystereses but also this temperature effect changes the shape of the stress–stretch curves, compare the loading–unloading curves at different strain levels, the same strain rate 0.1/s, and the same temperature in each graph. However, it does not mean that the nonlinearity modes are distinct at different temperatures. As is shown in Fig. 4, at room temperature when the specimen is loaded at a larger deformation up to 900% deformation, the stress–strain curve also demonstrates a strong nonlinearity similar to that at a lower temperature of −20 °C. In both cases, the slope of the curve bends down at a stretch of approximately 3 to a stable one, and tilts up at a stretch of approximately 7, although the strain range and stress

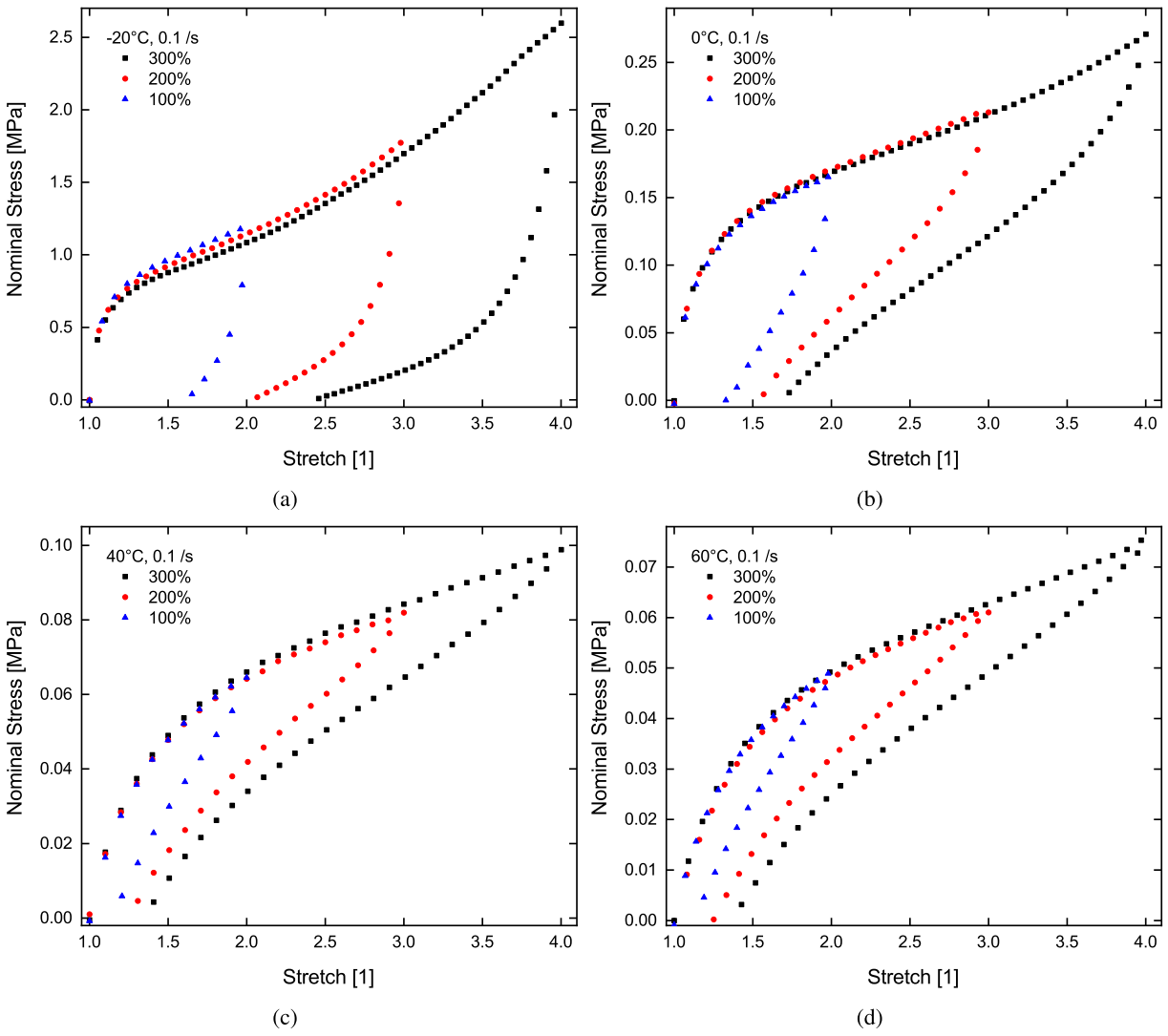

Fig. 5. Stress response and cyclic dissipation of three strain levels (100%, 200%, and 300%) with respect to temperature variations at a fixed strain rate of 0.1/s, (a) −20 °C, (b) 0 °C, (c) 40 °C, (d) 60 °C. These results demonstrate that the VHB 4905 becomes less dissipative with an increasing positive temperature.

levels are different between two temperature fields, −20 °C and 20 °C, respectively. Figs. 7 and 8 demonstrate the temperature dependence at 200% and 300% deformations, respectively, at the same strain rate of 0.1/s. As is shown, a lower temperature yields a higher stress level and a larger hysteresis with a larger residual strain, which is similar to the results of a higher strain rate. Moreover, we perform several cyclic tests with more than five cycles with a strain recovery period to reach the stress-free state, and it is revealed that the curves at all cycles overlap. That means there is no observed plasticity and damage such as the Mullins effect. Very recently, Fan and Szpunar [55] also presented similar observations for VHB. They found that the apparent 'Mullins effect' is almost recoverable after two hours of holding between the first cycle and the second cycle. Thus, the polymer is a purely viscoelastic material.

2.4. Single-step relaxation experiments

Single-step relaxation tests are used to determine the so-called basic elasticity, or in other words, the equilibrium stress response of polymeric materials. That means, for each test, the specimen is loaded at the maximum speed of the test machine and is held at a certain strain level. During that time, the sample is allowed to relax for three hours to reach an equilibrium stress. In our previous contributions, e.g. Hossain et al. [13], Mehnert and Steinmann [12], a thirty-minute period was taken as a holding time. However, to obtain a relaxed stress close to the equilibrium stress, a three-hour duration is taken as the relaxation time in the current study. Then the relaxed stress after a three-hour holding time of each strain level is considered as the equilibrium stress, which usually excludes the stress part generated by any polymeric viscosity.

Single-step relaxation experiments are performed on tensile specimens from 100% to 800% strains with an interval of 100% strains. For a better demonstration purpose, the stress history curves are shifted along the time axis to avoid overlapping of the curves, as is shown in Fig. 9(a). From the results, it can be observed that with time evolving, the stress attenuates to an equilibrium level. However, at a larger strain, it takes a longer time to relax. This implies that at a larger strain level, more relaxation time is required to obtain an equilibrium stress. Fig. 9(b) shows the loading curves with the relaxed stresses in a stress–strain format so that the amounts of relaxed stresses can clearly be visible. When the specimen is loaded to a certain strain level and is held there, the total stress (viscous over-stress plus the basic elastic stress) begins to drop gradually, and finally stabilizes at a certain point. At each strain level, there is a corresponding equilibrium stress (basic elastic stress). If all the relaxed stress points are connected, the so-called equilibrium (basic elasticity) path can be obtained.

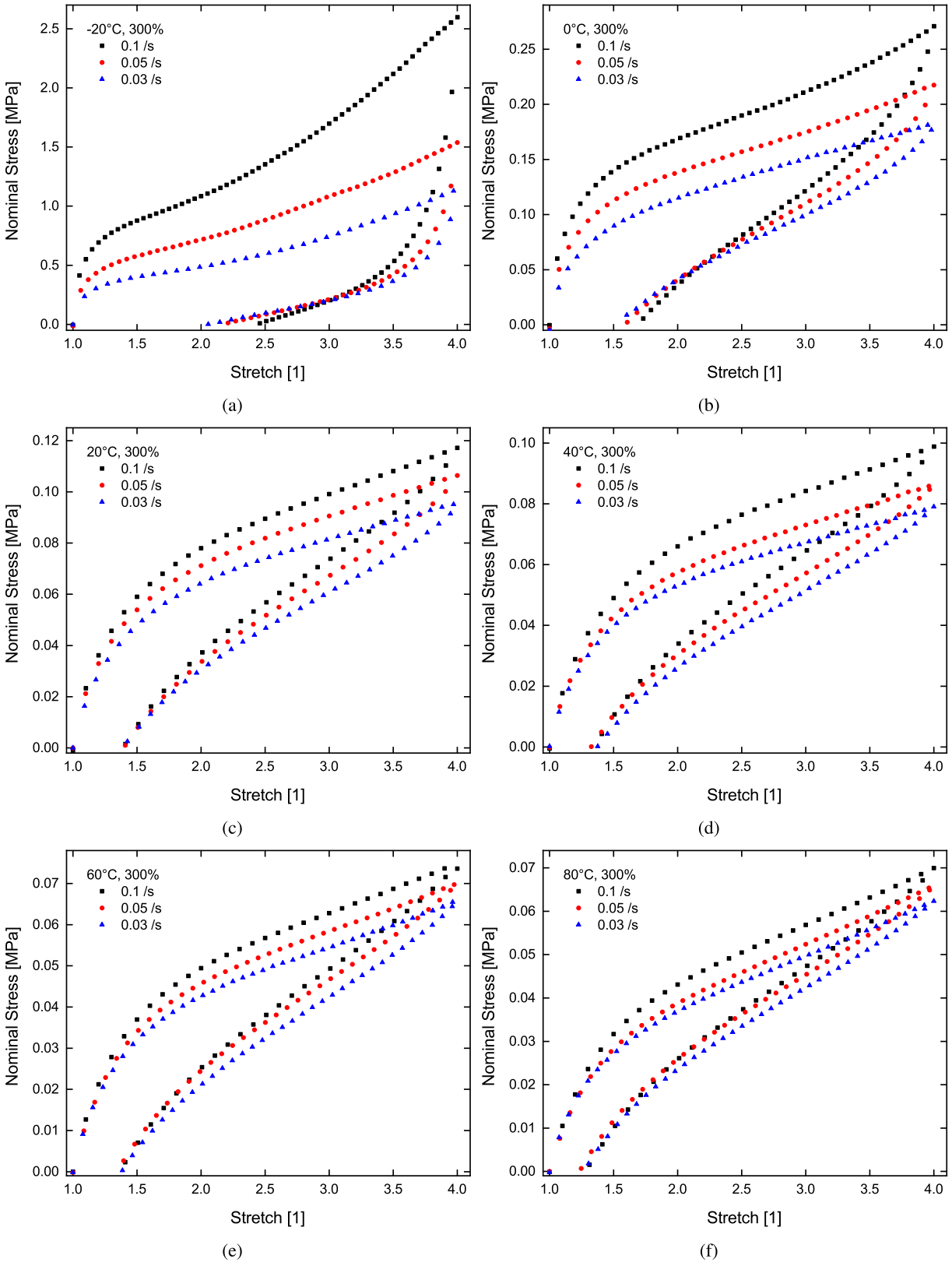

Fig. 6. Stress response with respect to different temperatures and strain rates (0.1/s, 0.05/s, and 0.03/s) at a fixed strain of 300%, (a) −20 °C, (b) 0 °C, (c) 20 °C, (d) 40 °C, (e) 60 °C, (f) 80 °C. As expected, VHB 4905 shows pronounced strain-rate dependence where a faster rate produces large stress and vice-versa.

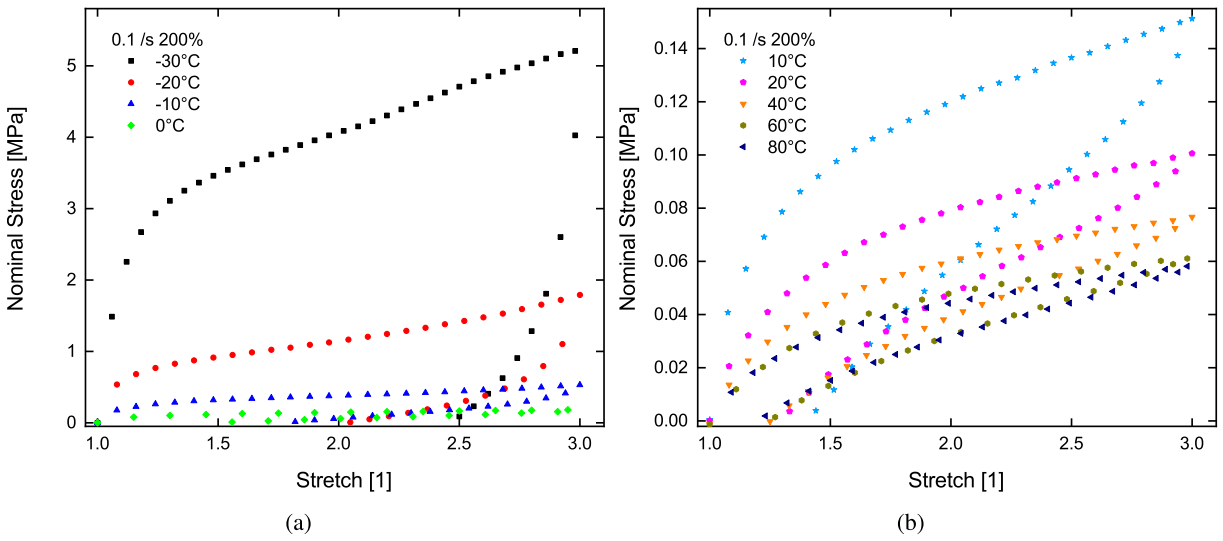

Fig. 7. Temperature-dependent stress response under a wide range of temperature where experiments are conducted at 200% strain and 0.1/s strain rate, (a) below 0 °C, (b) above 0 °C. All results clearly reveal that the temperature field has a major role in changing mechanical stress responses of the VHB polymer.

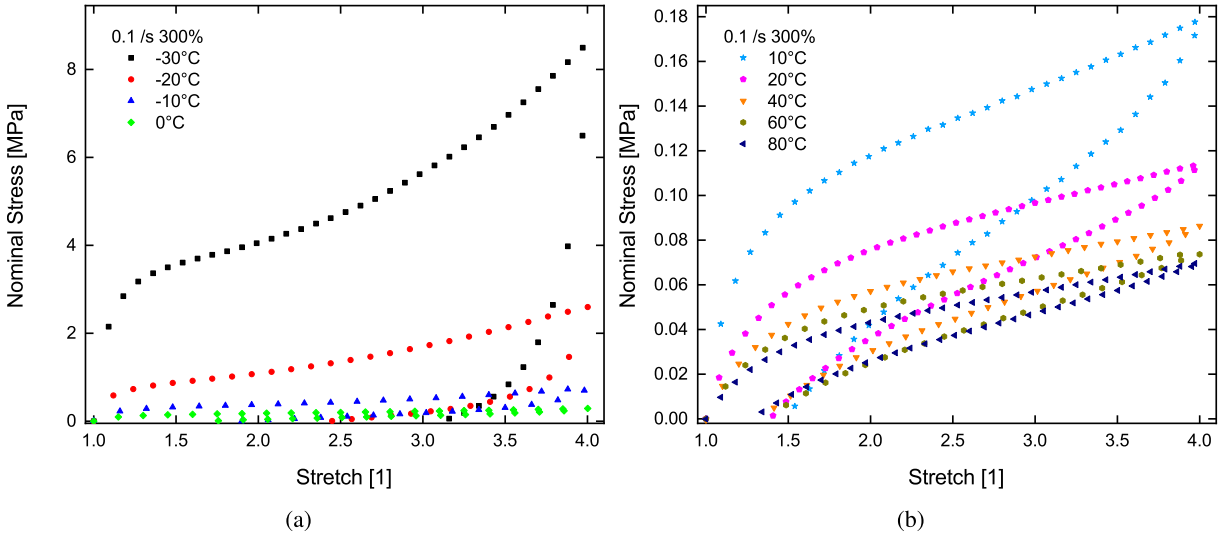

Fig. 8. Temperature-dependent stress response under a wide range of temperature where experiments are conducted at 300% strain and 0.1/s strain rate. (a) below 0 °C, (b) above 0 °C.

2.5. Multi-step relaxation experiments

Another way to identify the equilibrium stress of a polymeric material is the multi-step relaxation tests. Similar to the single-step relaxation experiments, the specimen is stretched to a certain strain level and is allowed to relax for a three-hour period before the specimen is re-loaded to the next strain level instead of being unloaded. In contrast to single-step relaxation experiments, in a multi-step relaxation test, several equilibrium stresses can be extracted only with the help of a single sample with a couple of steps in one test set-up. In this case, a multi-step relaxation experiment is carried out at increments of 100%, 300%, 500%, and 700% strains. As is shown in Fig. 10(a), the single-step relaxation tests and the corresponding steps of the multi-step relaxation tests share similar relaxation history curves with very close relaxed stresses (equilibrium stresses). Fig. 10(b) shows the loading curves in a stress–stretch form.

2.6. Quasi-static experiments

Furthermore, several quasi-static tensile tests at very slow strain rates (i.e., 0.0001/s) are also carried out. More tensile experiments at an even slower strain rate (i.e., 0.00001/s) are performed and it is observed that the latter results coincide with tests of 0.0001/s strain rate. Hence, the 0.0001/s strain rate is considered as the slowest strain rate for the quasi-static tensile tests. A single tensile experiment at such a low strain rate takes almost one day that allows a sample to sufficiently relax while it is being loaded. That means, the stress induced by any kind of viscosity will disappear and the loading curve can be regarded as the equilibrium (basic elasticity) path. Comparing the relaxed stresses of single-step and multi-step relaxation tests, it is found that they are almost identical. For a comparison purpose, single-step and multi-step relaxations and quasi-static test results are presented in Fig. 11 which will be used for the calibration of the equilibrium path.

In an effort to identify the effects of temperature on the equilibrium response of the VHB, we also perform a few more quasi-static tensile tests under various temperatures at the same strain rate of 0.0001/s. Note that these tests require a very long time, almost a day for only a single test. Therefore, regulating a specified temperature for such a long time is a cumbersome task. During the tests, several factors, e.g., perturbations by the air circulation, vibrations from the

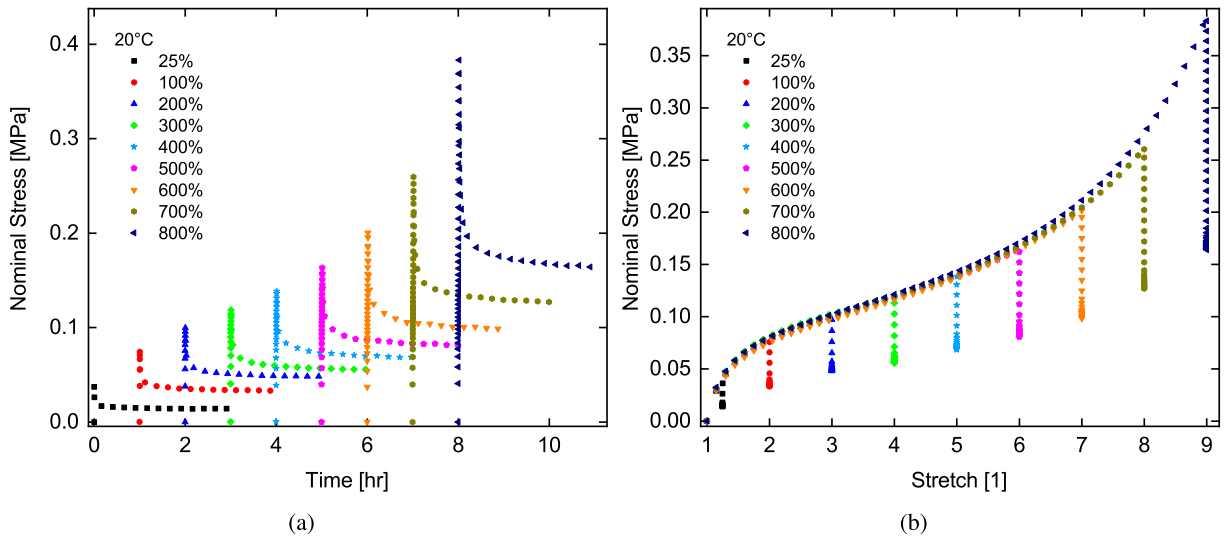

Fig. 9. Single-step relaxation test results from 25% to 800% strains. (a) Stress histories with respect to relaxation times, (b) Stress–strain curves depicting the amount of stress relaxations during the holding times.

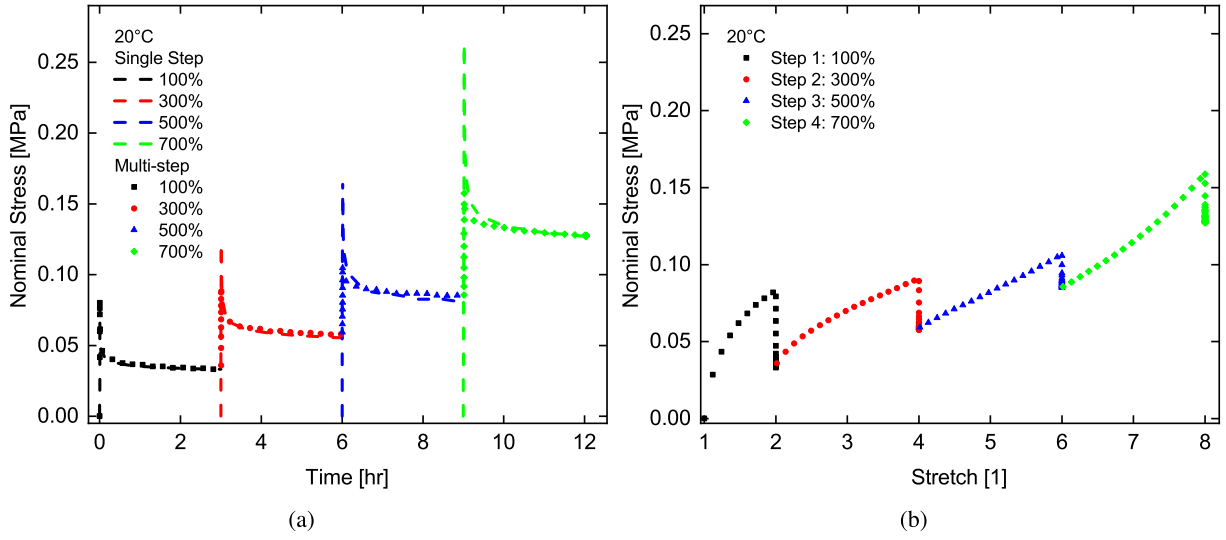

Fig. 10. Multi-step relaxation tests. (a) Intermittent stress history curves, (b) Stress–stretch curves depicting the amount of stress relaxations during holding times.

air-conditioning compressor, zero drift effects due to a temperature change of the stress sensor etc., create great risks which introduce strong oscillations and errors into some of the test results. Here, we only demonstrate an average of several successful tests after many unsuccessful quasi-static trials. The test at −20 °C of 500% deformation with a section of unloading exhibits a stable curve. Fig. 12 shows that at 500% deformation of the −20 °C test, the stress level (near 0.12 MPa) is only about 50% higher than that of 20 °C (slightly above 0.08 MPa). In contrast, at a 300% strain and 0.1/s strain rate tests, the stress level of −20 °C (near 2.6 MPa) is 2000% higher than that of 20 °C (about 0.11 MPa), as is shown in Fig. 8. Besides, the unloading path at −20 °C indicates that a sizeable hysteresis still exists, which means that the loading path of this test has not reached equilibrium yet. In fact, the relaxation time could be longer at a lower temperature. As a result, in order to reach the equilibrium path at −20 °C, the strain rate could be even smaller than that of 20 °C (i.e., 0.0001/s), which requires ten days or more time for only one test and is not practical in consideration of the aforementioned error factors. Hence, we tend to conclude that the temperature influence on the equilibrium path is negligible in comparison to the influence on the viscosity. Similar observations for other polymers have been documented in the literature, see Johlitz et al. [40], Dippel et al. [49], Koprowski et al. [38].

3. A thermo-viscoelastic model at finite strain

3.1. Kinematics

In order to consider a combination of mechanical and thermal loads, a multiplicative decomposition of the deformation gradient $\boldsymbol{F}$ into a thermal part $\boldsymbol{F}_\Theta$ and a mechanical deformation $\boldsymbol{F}_M$ is introduced as

$$\boldsymbol{F} = \boldsymbol{F}_M \boldsymbol{F}_\Theta. \tag{1}$$

For more details about this approach, see Lu and Pister [56], Reese [34], Lion [20], Erbts et al. [57]. Furthermore, to capture the time-dependent viscoelastic response at finite strains, a multiplicative decomposition of the deformation gradient is frequently used as

$$\boldsymbol{F} = \boldsymbol{F}_M \boldsymbol{F}_\Theta = \boldsymbol{F}_M^{\mathrm{vol}} \boldsymbol{F}_M^{\mathrm{iso}} \boldsymbol{F}_\Theta = \boldsymbol{F}_M^{\mathrm{vol}} \boldsymbol{F}_{M,e}^{j} \boldsymbol{F}_{M,v}^{j} \boldsymbol{F}_\Theta \tag{2}$$

where $j = 1 \dots n$ is related to the possibility of multiple viscous mechanisms with each one represented by a Maxwell element. Note that viscous responses are assumed to be isochoric only, see Reese and Govindjee [34], Dippel et al. [49], Miehe et al. [28]. Furthermore, we can use the deformation gradient $\boldsymbol{F}$ for the definition of the right Cauchy–Green tensor $\boldsymbol{C} = \boldsymbol{F}^T \boldsymbol{F}$. The corresponding elastic and inelastic

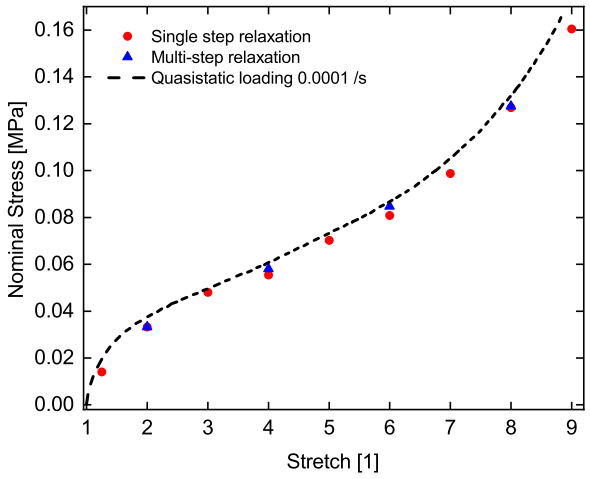

Fig. 11. Comparison of relaxed equilibrium stresses obtained from single-step relaxation experiments (•), from multi-step relaxation tests (△), and from quasi-static tests (––) up to 800% strains. Equilibrium stresses from three different sets of experiments match very closely.

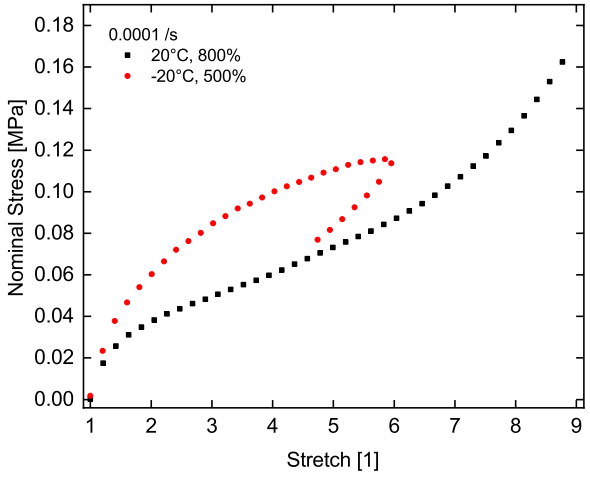

Fig. 12. Quasi-static tensile experiments at a 0.0001/s strain rate at different temperatures to illustrate the influences of temperature on the equilibrium stress responses: After couple of unsuccessful tests, two successful experiments at −20 °C and 20 °C are presented which show that the temperature has a minor influence on the elastic stress compared to the total viscoelastic stress.

right Cauchy–Green strain tensors are defined as $\boldsymbol{C}^j_{M,e} = [\boldsymbol{F}^j_{M,e}]^T \boldsymbol{F}^j_{M,e}$ and $\boldsymbol{C}^j_{M,v} = [\boldsymbol{F}^j_{M,v}]^T \boldsymbol{F}^j_{M,v}$, respectively. We here introduce the thermal expansion coefficient α and the temperature difference $(\Delta\Theta = \Theta - \Theta_0)$ which results in the decomposition of the Jacobian determinant into

$$J = \det \boldsymbol{F} = \det \boldsymbol{F}_M \ \det \boldsymbol{F}_\Theta = J_M J_\Theta, \tag{3}$$

where the thermal Jacobian is scaled either with an exponential function as $J_\Theta = \exp(3\alpha\Delta\Theta)$ or with a linear function, i.e., $J_\Theta = \alpha\Delta\Theta + 1$, see Dippel et al. [49], Erbts et al. [57]. Furthermore, the definition of the isochoric right Cauchy–Green tensor is $\overline{\boldsymbol{C}} = J^{-\frac{2}{3}}\boldsymbol{C}$. As the thermal expansion is purely volumetric it holds that the isochoric Cauchy–Green tensor capturing the combined deformation is equal to the mechanical contribution, i.e.

$$\overline{\boldsymbol{C}} = \overline{\boldsymbol{C}}_\Theta \overline{\boldsymbol{C}}_M = \overline{\boldsymbol{C}}_M. \tag{4}$$

Finally, as rubber-like materials can be assumed to be incompressible at a constant temperature the decomposition between the mechanical and the thermal deformation resembles a decomposition into a purely isochoric and a purely volumetric deformation. In this case, we can state that

$$J_M = 1 \quad \text{and} \quad J = J_\Theta. \tag{5}$$

3.2. A thermo-viscoelastic energy function

In an effort to derive a generic energy function for thermo-viscoelastic polymers, in our previous contributions the specific heat capacity is assumed to be temperature independent, i.e. $c(\Theta) = c_0 = \text{const}$, see Mehnert et al. [16]. Departing from the definition of $c(\Theta) = -\Theta\frac{\partial^2\Psi}{\partial\Theta\partial\Theta}$, a full derivation of the energy function $\Psi(\boldsymbol{F},\Theta)$ can be obtained where a linear scaling of the isothermal energy contribution $W_0(\boldsymbol{F}_M)$ is produced with the temperature in the form

$$\Psi(\boldsymbol{F},\Theta) = \frac{\Theta}{\Theta_0} W_0(\boldsymbol{F}_M) - \Big[\Theta - \Theta_0\Big] M(J_\Theta) - c_0\Big[\Theta - \Theta_0 - \Theta\ln\Big(\frac{\Theta}{\Theta_0}\Big)\Big], \tag{6}$$

where $M(J_\Theta)$ describes the purely volumetric thermal expansion of the material. However, it is well documented in the literature that the key mechanical material parameters such as the shear modulus and the bulk modulus exhibit nonlinear dependencies with respect to the temperature, see Treloar [58], Nowinski [59], Johlitz et al. [39,40]. Therefore, Reese and Govindjee [34], Benhke et al. [48] formulated a generalized and realistic energy function by taking an advanced definition of the specific heat capacity that depends on temperature in the form as

$$c(\Theta) = c_0 - \Theta\frac{\partial^2 g(\Theta)}{\partial\Theta^2} W_0(\boldsymbol{F}_M), \tag{7}$$

where $g(\Theta)$ is a temperature sensitive scaling function. A double integration of the above equation with applications of appropriate initial and boundary conditions result in a nonlinear relation between the temperature and the energy function in the form

$$\Psi = \left[\frac{\Theta}{\Theta_0} + g(\Theta)\right] W_0(\boldsymbol{F}_M) - \Big[\Theta - \Theta_0\Big] M(J_\Theta) - c_0\Big[\Theta - \Theta_0 - \Theta\ln\Big(\frac{\Theta}{\Theta_0}\Big)\Big]. \tag{8}$$

For modelling thermo-viscoelastic material behaviour, it is a common practice to decompose the isothermal energy contribution $W_0(\boldsymbol{C}_M)$ into an isochoric contribution $\widetilde{W}_{\text{iso}}(\overline{\boldsymbol{C}}_M, \boldsymbol{C}^j_{M,v})$ and a volumetric contribution $\widetilde{W}_{\text{vol}}(J_M)$ where the latter vanishes if we consider the material to be incompressible at a constant temperature. Note that $\widetilde{W}_{\text{iso}}(\overline{\boldsymbol{C}}_M, \boldsymbol{C}^j_{M,v})$ depends not only on the deformation gradient but also on a number of tensorial internal variables $\boldsymbol{C}_{M^j,v}$. The subscript j $(j_{1\ldots N})$ is related to the possibility of multiple viscous mechanisms.

In the next step, the isochoric energy is further decomposed into an elastic part $\widetilde{W}^e_{\text{iso}}(\overline{\boldsymbol{C}}_M)$ and a viscous contribution $\widetilde{W}^v_{\text{iso}}(\overline{\boldsymbol{C}}_M, \boldsymbol{C}^j_{M,v})$ that captures the time dependent behaviour [21,22]. In order to gauge both the elastic and the viscous energy contributions independently from each other, we also transform the specific heat capacity into a form that contains separate scaling functions $g^e(\Theta)$ and $g^v(\Theta)$ which are multiplied with the respective energy contribution, resulting in

$$c(\Theta) = c_0 - \Theta\frac{\partial^2 g^e(\Theta)}{\partial\Theta^2}\widetilde{W}^e_{\text{iso}}(\overline{\boldsymbol{C}}_M) - \Theta\frac{\partial^2 g^v(\Theta)}{\partial\Theta^2}\widetilde{W}^v_{\text{iso}}(\overline{\boldsymbol{C}}_M, \boldsymbol{C}^j_{M,v}). \tag{9}$$

Note that several scaling functions, both for the elastic and viscous parts, exist in the literature, see [16,34,48,52]. An appropriate choice of the scaling functions depends on the experimental data of a particular polymer. These modifications ultimately lead to a full-scale thermo-viscoelastic energy function of the form

$$\begin{aligned}\Psi = &\left[\frac{\Theta}{\Theta_0} + g^e(\Theta)\right]\widetilde{W}^e_{\text{iso}}(\overline{\boldsymbol{C}}_M) + \left[\frac{\Theta}{\Theta_0} + g^v(\Theta)\right]\widetilde{W}^v_{\text{iso}}(\overline{\boldsymbol{C}}_M, \boldsymbol{C}^j_{M,v}) \\ &- \Big[\Theta - \Theta_0\Big] M(J_\Theta) - c_0\Big[\Theta - \Theta_0 - \Theta\ln\Big(\frac{\Theta}{\Theta_0}\Big)\Big]\end{aligned} \tag{10}$$

which can be considered as a combination of four separate energy functions, i.e., $\Psi = \Psi^e_{\text{iso}} + \Psi^v_{\text{iso}} + \Psi_{\text{vol}} + \Psi^e_{\text{th}}$.

3.3. Three-dimensional stresses for thermo-viscoelasticity

A decoupled formulation of the total energy function in the case of a nearly-incompressible material motivates a decomposition of the stress tensor into an isochoric part and a volumetric part. Hence, the mechanical stress tensor is decomposed as

$$\boldsymbol{S}_M = \boldsymbol{S}_{\text{vol}} + \boldsymbol{S}_{\text{iso}} = 2\frac{\partial \Psi_{\text{vol}}}{\partial \boldsymbol{C}_M} + 2\frac{\partial \Psi_{\text{iso}}}{\partial \boldsymbol{C}_M}, \tag{11}$$

where $\boldsymbol{S}_{\text{vol}} = J_M p \boldsymbol{C}_M^{-1}$ is the volumetric part of the stress and $p = \partial \Psi_{\text{vol}}(J_M)/\partial J_M$ is the hydrostatic pressure. Note that for a fully incompressible material $J_M = 1$ and p serves as a Lagrange multiplier. In order to obtain the isochoric stress $\boldsymbol{S}_{\text{iso}}$ from the energy function Ψ_{iso}, another stress $\bar{\boldsymbol{S}}_M = 2\partial \Psi_{\text{iso}}(\bar{\boldsymbol{C}}_M, \boldsymbol{C}_v)/\partial \bar{\boldsymbol{C}}_M$ is introduced which is related to the former one via a fourth-order projection tensor $\mathbb{P} = \partial \bar{\boldsymbol{C}}_M / \partial \boldsymbol{C}_M$ by

$$\boldsymbol{S}_{\text{iso}} = J^{-\frac{2}{3}} \mathbb{P} : \bar{\boldsymbol{S}}_M \qquad \text{with} \qquad \mathbb{P} = \mathbb{I} - \frac{1}{3}\boldsymbol{C}_M^{-1} \otimes \boldsymbol{C}_M \quad , \quad \mathbb{I}_{ijkl} = \delta_{ik}\delta_{jl} \tag{12}$$

where δ_{ij} is a Kronecker delta. The stress $\bar{\boldsymbol{S}}_M$ is further decomposed into elastic and viscous parts, i.e. $\bar{\boldsymbol{S}}_M = \bar{\boldsymbol{S}}_M^e + \bar{\boldsymbol{S}}_M^v$. Each stress mentioned above requires a separate energy function to have a complete representation. For the ground state elasticity, the Carrol [60] model is chosen since it has shown excellent performance in fitting hyperelastic experimental data of polymeric materials with only three material parameters, see Steinmann et al. [61], Hossain et al. [11,62,63]. Hence, a Carrol-type energy function is scaled with a temperature-dependent factor as

$$\Psi_{\text{iso}}^e(\bar{\boldsymbol{C}}_M, \Theta) = \left[\frac{\Theta}{\Theta_0} + g^e(\Theta)\right]\left[a\bar{I}_1 + b\bar{I}_1^4 + c\sqrt{\bar{I}_2}\right], \tag{13}$$

where a, b, c are the material parameters and $\bar{I}_1$, $\bar{I}_2$ are the first and second invariants of the isochoric right Cauchy–Green tensor $\bar{\boldsymbol{C}}_M$. From Eq. (11) and using the relation in (13), the elastic part of the stress tensor can be calculated:

$$\bar{\boldsymbol{S}}_M^e = 2\frac{\partial \Psi_{\text{iso}}^e}{\partial \bar{\boldsymbol{C}}_M} = \left[\frac{\Theta}{\Theta_0} + g^e(\Theta)\right]\left[[2a + 8b\bar{I}_1^3]\boldsymbol{I} + c[\bar{I}_1\boldsymbol{I} - \bar{\boldsymbol{C}}_M]\bar{I}_2^{1/2}\right], \quad \boldsymbol{I} \equiv \delta_{ij}. \tag{14}$$

For the viscous part of the energy function, we take the approach formulated by Koprowski et al. [37,38], Dippel et al. [49], Scheffer et al. [50], Sedlan [47] that yields nonlinear evolution laws. In order to capture more complex experimental data presented in Section 2, we take two different non-equilibrium energy functions in the viscous part. In this case, the first part is derived from a higher order Yeoh model of cubic type and the second part is from a Neo-Hooke energy function as

$$\Psi_{\text{iso}}^v(\bar{\boldsymbol{C}}_{M,e}, \Theta) = \sum_{j=1}^{2}\Psi_Y^{v,j} + \sum_{j=3}^{5}\Psi_{NH}^{v,j} = \sum_{j=1}^{2} c_4^j[I_{1,e}^j - 3]^3 + \sum_{j=3}^{5} c_5^j[I_{1,e}^j - 3], \tag{15}$$

where c_4^j and c_5^j are material constants with each Maxwell spring's element. Note that $I_{1,e}^j$ is the first invariant of $\bar{\boldsymbol{C}}_{M,e}^j$, i.e., $I_{1,e}^j = \text{tr}(\bar{\boldsymbol{C}}_{M,e}^j) = \text{tr}(\boldsymbol{F}_{M,v}^{-T} \dots \bar{\boldsymbol{C}}_M \dots \boldsymbol{F}_{M,v}^{-1})$. Afterwards, the non-equilibrium viscous stress is defined as

$$\bar{\boldsymbol{S}}_M^v = 2\frac{\partial \Psi_{\text{iso}}^v}{\partial \bar{\boldsymbol{C}}_M} = \left[\frac{\Theta}{\Theta_0} + g^v(\Theta)\right] \times \left[\sum_{j=1}^{2} 6c_4^j[I_{1,e}^j - 3]^2[\boldsymbol{C}_{M,v}^j]^{-1} + \sum_{j=3}^{5} 2c_5^j[\boldsymbol{C}_{M,v}^j]^{-1}\right], \tag{16}$$

where $\boldsymbol{C}_{M,v}^j$ is a tensorial internal variable related to a Maxwell element. For this, an evolution equation can be derived as

$$\dot{\boldsymbol{C}}_{M,v}^j = \frac{4}{\eta^j}\frac{\partial \Psi_{\text{iso}}^{v,j}}{\partial I_{1,e}^j}\left[\boldsymbol{C}_M - \frac{1}{3}\left[\boldsymbol{C}_M : [\boldsymbol{C}_{M,v}^j]^{-1}\right]\boldsymbol{C}_{M,v}^j\right], \tag{17}$$

where a proportionality factor η^j is introduced representing the viscoelasticity of the jth Maxwell element. For the proof of the thermodynamical consistency and a detailed derivation of the above equation, see Koprowski et al. [37,38], Scheffer et al. [50], Saxena et al. [31]. Note that we have two energy functions in the non-equilibrium viscous part, cf. Eq. (15). Hence, according to Eq. (17), they will end up with two evolution equations as the first one, using the Yeoh-type non-equilibrium energy function $(15)_1$, becomes

$$\dot{\boldsymbol{C}}_{M,v}^j = \frac{12}{\tau_1^j}[I_{1,e}^j - 3]^2\left[\boldsymbol{C}_M - \frac{1}{3}\left[\boldsymbol{C}_M : [\boldsymbol{C}_{M,v}^j]^{-1}\right]\boldsymbol{C}_{M,v}^j\right], \quad j = 1 \dots 2, \quad \tau_1^j = \frac{\eta^j}{c_4^j} \tag{18}$$

and the second equation from the Neo-Hooke non-equilibrium function $(15)_2$ yields

$$\dot{\boldsymbol{C}}_{M,v}^j = \frac{4}{\tau_2^j}\left[\boldsymbol{C}_M - \frac{1}{3}\left[\boldsymbol{C}_M : [\boldsymbol{C}_{M,v}^j]^{-1}\right]\boldsymbol{C}_{M,v}^j\right], \quad j = 3 \dots 5, \quad \tau_2^j = \frac{\eta^j}{c_5^j}. \tag{19}$$

3.4. One-dimensional constitutive models for thermo-viscoelasticity

Since all of the results presented in Section 2 are produced from a homogeneous mode of deformation, the constitutive model discussed above needs to be reformulated in a one-dimensional form in order to identify the material parameters as well as to validate the applied model. In uniaxial tests, the specimen is elongated only in one direction, i.e., $\lambda_1 = \lambda$ while the other two directions are free to move. From the incompressibility condition at fixed temperature, i.e., $\det\boldsymbol{F} = \det\bar{\boldsymbol{F}} = \det\boldsymbol{F}_v = \det\boldsymbol{F}_\Theta = 1$, i.e., $\lambda_1\lambda_2\lambda_3 = 1$ and the assumption of symmetry the complementary principal stretches follow as $\lambda_2 = \lambda_3 = \lambda^{-1/2}$. Therefore, the complete deformation gradient reads $\boldsymbol{F} = \{\lambda; \lambda^{-1/2}; \lambda^{-1/2}\}$. Note that since the elongation is only in one direction, the specimen will contract in the transversal directions and due to the stress-free boundary conditions, both Piola stresses P_2 and P_3 are zero and only the Piola stress P_1 needs to be determined. Inserting all this information in Eq. (14), the elastic part of the Piola stress is obtained:

$$P^e = \left[\frac{\Theta}{\Theta_0} + g^e(\Theta)\right]\left[2a + 8b[2\lambda^{-1} + \lambda^2]^3 + c[1 + 2\lambda^3]^{-\frac{1}{2}}\right][\lambda - \lambda^{-2}] \tag{20}$$

for details, see Hossain [13], Steinmann et al. [61]. Note that since we have observed negligible influence of the temperature on the equilibrium response during our study, $g^e(\Theta) = 1 - \frac{\Theta}{\Theta_0}$ is taken here. Now, the viscous part of the stress for a single Maxwell element is formulated (assuming incompressibility for the internal variable $\boldsymbol{C}_v$) from Eq. (16):

$$\begin{aligned} P^v &= \left[\frac{\Theta}{\Theta_0} + g_1^v(\Theta)\right]\sum_{j=1}^{2} P^{v,j} + \left[\frac{\Theta}{\Theta_0} + g_2^v(\Theta)\right]\sum_{j=3}^{5} P^{v,j} \\ &= \left[\frac{\Theta}{\Theta_0} + g_1^v(\Theta)\right]\sum_{j=1}^{2} 6c_4^j\left[\frac{\lambda^2}{[\lambda_v^j]^2} + \frac{2\lambda_v^j}{\lambda} - 3\right]^2\left[\frac{\lambda}{[\lambda_v^j]^2} - \frac{\lambda_v^j}{\lambda^2}\right] \\ &\quad + \left[\frac{\Theta}{\Theta_0} + g_2^v(\Theta)\right]\sum_{j=3}^{5} 2c_5^j\left[\frac{\lambda}{[\lambda_v^j]^2} - \frac{\lambda_v^j}{\lambda^2}\right], \end{aligned} \tag{21}$$

where λ_v^2 is the principal stretch of the internal variable $\boldsymbol{C}_v$. Similar to the one-dimensional formulation of the total stress, the first evolution law (18) is derived:

$$\dot{\lambda}_v^j = \frac{4}{\tau_1^j}\left[\frac{\lambda^2}{[\lambda_v^j]^2} + \frac{2\lambda_v^j}{\lambda} - 3\right]^2\left[\frac{\lambda^2}{\lambda_v^j} - \frac{[\lambda_v^j]^2}{\lambda}\right], \qquad j = 1, 2 \tag{22}$$

and the one-dimensional form of the second evolution equation (19) is

$$\dot{\lambda}_v^j = \frac{4}{3\tau_2^j}\left[\frac{\lambda^2}{\lambda_v^j} - \frac{[\lambda_v^j]^2}{\lambda}\right], \qquad j = 3 \dots 5. \tag{23}$$

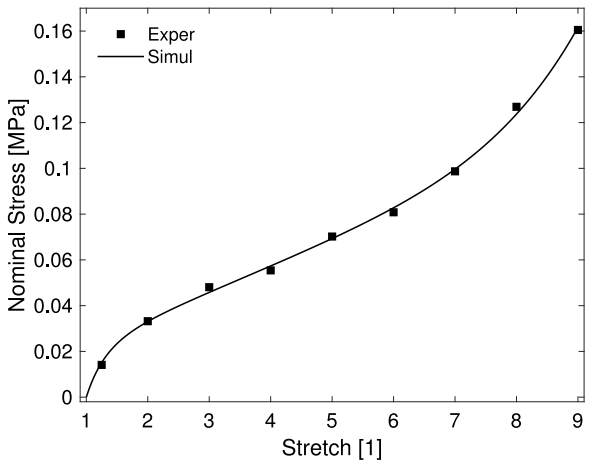

Fig. 13. Parameter identification: Hyperelastic material parameters of the Carrol model identified by the quasi-static experimental data measured at the reference temperature (20 °C).

Now both the scalar-valued differential equations need to be discretized by a suitable integration scheme. Discretizing by the unconditionally stable implicit Euler-backward integration scheme, the differential equation for the internal variable λ_v^j for a single Maxwell element yields

$$\lambda_v^j = \lambda_v^{j,n} + \frac{4\Delta t}{3\tau_2^j}\left[\frac{\lambda^2}{\lambda_v^j} - \frac{[\lambda_v^j]^2}{\lambda}\right], \tag{24}$$

where $[\bullet]^k = [\bullet](t_k)$ and $\Delta t = t_{n+1} - t_n$. For the sake of brevity, the index for the current value (t_{n+1}) of the stretch λ_v^j has been dropped in Eq. (24). Eq. (24) is non-linear in terms of λ_v^j. Therefore, a Newton-type iterative scheme is required to find the current value of λ_v^j that need to be inserted in Eq. (21) to obtain the updated value of the total Piola stress, $P(t) = P^e + P^v(t)$.

4. Parameter identification and model validation

4.1. Hyperelastic parameter identification at the reference temperature

For the identification of hyperelastic material parameters appearing in a constitutive model, three main procedures have been discussed in the literature, see Koprowski et al. [37,38], Johlitz et al. [39,40], Hossain et al. [13]. The first option is to perform single-step relaxation experiments at various strain levels. When a test specimen is held at a certain strain, the stress will gradually reduce and will asymptotically reach an equilibrium stress state, which can be considered as the relaxed and basic elastic stress at the corresponding strain. The second option for identifying equilibrium stresses and subsequent parameter identification is to conduct multi-step relaxation experiments. In contrast to single-step relaxation tests, in multi-step experiments, the equilibrium stresses are extracted from one specimen at consecutive steps of strains and stress relaxations.

The third option is to apply a monotonic quasi-static loading at a sufficiently slow strain rate. To find such a slow strain rate, an iterative technique needs to be applied. For that, quasi-static tests are performed at several consecutively decreasing slow strain rates. If the corresponding stress does not decrease despite the decreasing strain rates, such a strain rate is considered as an optimum strain rate for quasi-static tests. At such a very low strain rate, all viscosity is considered to have disappeared and only hyperelastic (equilibrium) stresses will remain. Since all three types of tests reflect the same equilibrium path, their equilibrium stresses at a particular strain should ideally be identical or very close to each other, and that is the case in Fig. 11. These almost identical results reflect the reproducibility and accuracy of our experiments under different types of test procedures. Since experimental data from three different sources almost coincide with each other, we choose the quasi-static test data for a subsequent parameter identification as they consist of more data points. Therefore, the quasi-static data are fitted to the Carrol model for the parameter identification by Eq. (20). The identified parameters are shown in Table 1, and the fitting result is shown in Fig. 13. Despite the fact that the equilibrium path at the reference temperature exhibits a strong nonlinearity with a complex 'S' shape curve, the employed Carrol model fits the data perfectly. The scaling function g^e can be identified based on the one successful data at −20 °C as is shown in Fig. 12. However, its validation at another temperature is not possible at this stage. This is due to a lack of further data under the extreme complexities in conducting temperature-dependent experiments at very slow strain rates, see discussion in Section 2.6. Moreover, the identified values of g^e based on the equilibrium data at −20 °C is insignificant in compared to g^v. Hence, it is concluded in this study that the elastic part of the model is not influenced by a temperature change, i.e., $g^e(\Theta) = 1 - \frac{\Theta}{\Theta_0}$ in Eq. (20).

Table 1
Hyperelastic parameters identified with the quasi-static data by Carrol model.

a [MPa]	b [MPa]	c [MPa]
6.018e−03	1.215e−09	2.820e−02

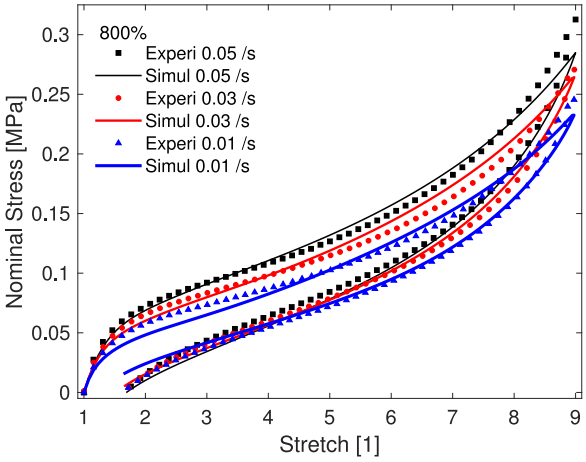

Fig. 14. Viscoelastic parameter identification: Three different strain rates are used to identify viscous parameters while the hyperelastic parameters identified earlier are kept frozen. Five Maxwell elements (2 Yeoh and 3 Neo-Hooke), each having two material parameters, are well enough to capture the strain rate-dependent data up to 800% strains.

4.2. Viscoelastic parameter identification and validation at the reference temperature

The next step is to identify the viscoelastic parameters. With the hyperelastic parameters, the equilibrium stress can be calculated, and the over-stress modulus c_i^j and over-stress relaxation spectrum τ_i^j are yet to be identified in order to obtain the viscous over-stress. Since the viscoelastic phenomenon has a strain rate-dependent behaviour, we identify the parameters using three sets of data at 800% strain and at different strain rates, which are 0.01/s, 0.03/s, and 0.05/s, simultaneously. Note that during the identification process, we find that five Maxwell elements (2 Yeoh and 3 Neo-Hooke) can capture the viscoelastic behaviour with a fair accuracy while more elements could not improve the results significantly. During the viscoelastic parameter identification, the hyperelastic parameters appearing in Table 1 are kept frozen. For the viscoelastic parameter identification, Eqs. (20) and (21) are jointly fitted with experimental data and the identified

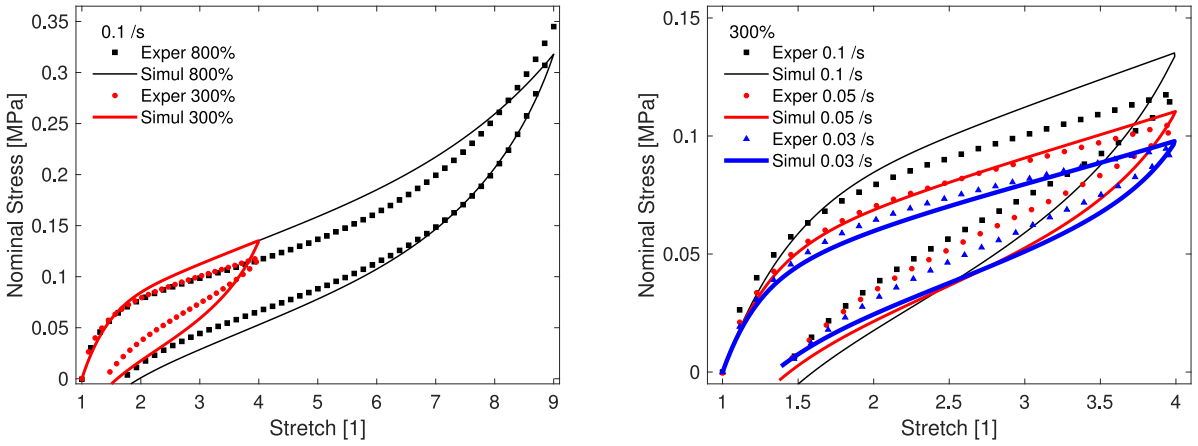

Fig. 15. Viscoelastic model validation at the reference temperature : (a) 300% and 800% strains data are used with a strain rate of 0.1/s, (b) 300% strain data are used at three different strain rates (0.1/s, 0.05/s, 0.03/s).

Table 2
Viscoelastic parameters at the reference temperature: Two Maxwell elements with a Yeoh type non-equilibrium energy function.

c_4^1 [MPa]	τ_1^1 [s]	c_4^2 [MPa]	τ_1^2 [s]
3.227e−05	3.048e+02	1.630e−10	3.954e−04

Table 3
Viscoelastic parameters at the reference temperature: Three Maxwell elements with a Neo-Hooke type non-equilibrium energy function.

c_5^3 [MPa]	τ_2^3 [s]	c_5^4 [MPa]	τ_2^4 [s]	c_5^5 [MPa]	τ_2^5 [s]
1.327e−02	3.427e+01	2.115e−03	5.403e+02	4.503e−04	1.233e+05

parameters are shown in Tables 2 and 3. Simulation results produced by the identified parameters are shown in Fig. 14. Both strain rate dependence and large strain nonlinearities are captured successfully.

Now a complete set of viscoelastic parameters is identified at the reference temperature (room temperature), see Tables 1–3. Afterwards, the applicability of the viscoelastic model needs to be checked by predicting other test conditions which are not included in the parameter identification process. Firstly, an extended strain rate 0.1/s, which is not included in the identification process, is selected at 300% and 800% strains as is shown in Fig. 15(a). Comparing the simulation results and experimental data, it can be seen that the model can predict the data quite well even for such large deformations. Furthermore, the model is simulated with three strain rates (0.1/s, 0.05/s, and 0.3/s) at a 300% strain which clearly demonstrates that it can predict a wide range of strain rates and strains, cf. Fig. 15(b). Only a small discrepancy occurs at 300% where the stress levels predicted by the model are slightly higher than the experiments. Besides the cyclic test simulations mentioned above, few single-step relaxation tests are also simulated at 100%, 300%, 500%, and 700% strains. As is shown in Fig. 16, the relaxation behaviour including relaxation time and relaxation stresses can be predicted with an excellent agreement between experimental data and model predictions.

4.3. Viscoelastic parameter identification and validation at various temperatures

After the parameter identification at room temperature (reference temperature), the next step is to identify the influence of temperature by the scaling functions appearing in the model, i.e., g_1^v and g_2^v in Eq. (21). It is already mentioned that the temperature has a negligible influence on the equilibrium response. Hence, we just need to identify the scaling functions g_1^v and g_2^v. After several trial and errors, the

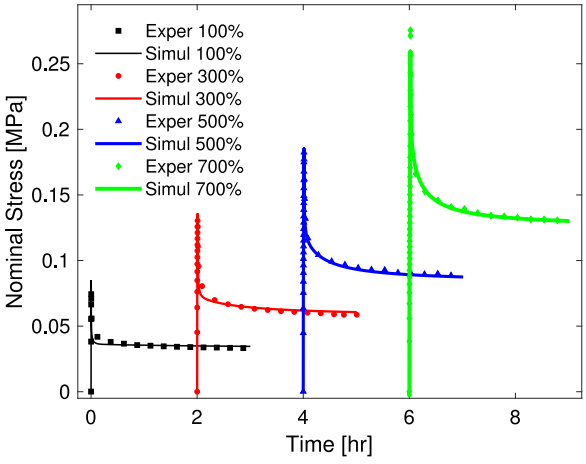

Fig. 16. Viscoelastic model validation at the reference temperature : Model validations with single-step relaxations data show an excellent agreement between the model and experiments.

Table 4
Temperature-responsive viscoelastic parameters.

a_T [1]	b_T [1]	c_T [1]
1.931e+01	2.120e−01	2.076e+01

following functions are best fitted to the experimental data,

$$g_1^v(\Theta) = -\frac{\Theta}{\Theta_0} + \exp\Big(\Big[\frac{\Theta_0}{\Theta_0 - 40}\Big]^{C_T} - \Big[\frac{\Theta}{\Theta_0 - 40}\Big]^{C_T}\Big);$$
$$g_2^v(\Theta) = -\frac{\Theta}{\Theta_0} + \frac{\exp(a_T \frac{\Theta_0}{\Theta} \ln \frac{\Theta_0}{\Theta}) + b_T}{1 + b_T} \tag{25}$$

where a_T, b_T, c_T are parameters that are identified from a set of temperature-dependent viscoelastic data. Based on the data of 300% strain and −20 °C, 20 °C, and 60 °C temperatures, parameters appearing in the scaling functions are identified as in Table 4 and the fitting results are shown in Fig. 17. It is clear that with a decrease in temperature, the stress level increases exponentially, and our model can capture such significant temperature-dependent effects quite well despite a very high variation in the stress level.

The final step is to validate the model at other temperature conditions. Firstly, 80 °C and 0 °C cyclic tests at 100%, 200%, and 300% strains are validated and results are illustrated in Fig. 18(b) which show a good agreement between the model simulation and experimental data. At 0 °C, it is shown in Fig. 18(a) that although their stress levels

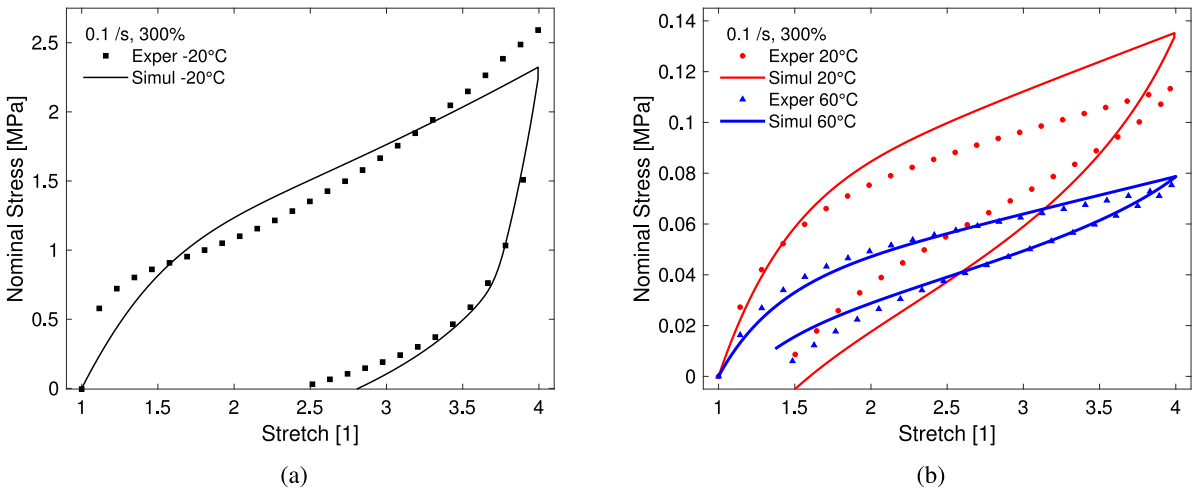

Fig. 17. Thermo-viscoelastic parameter identification taking into account of a wide range of temperature data from −20 °C to 60 °C with a strain of 300% and a strain rate of 0.1/s: (a) −20 °C, (b) 20 °C and 60 °C.

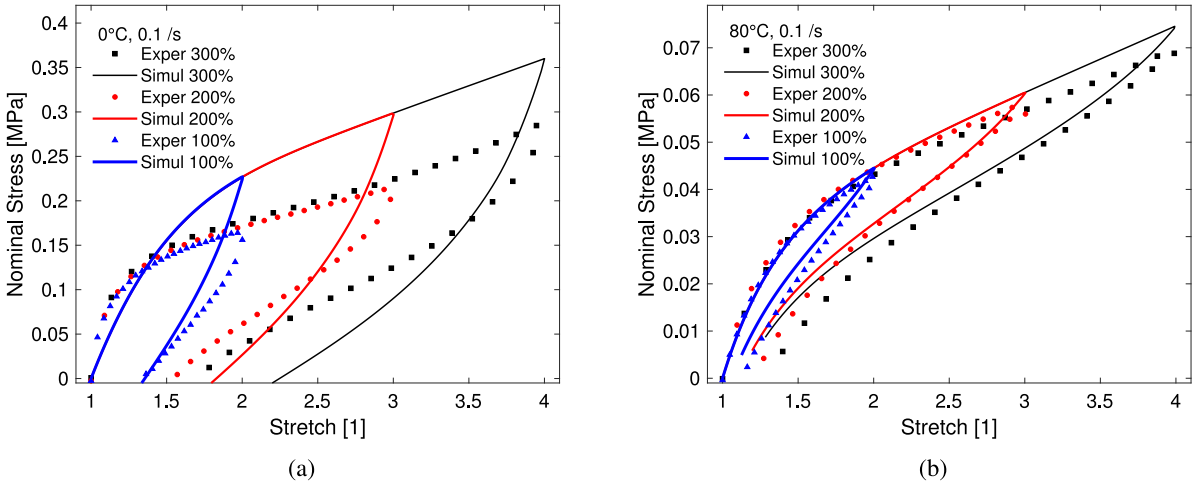

Fig. 18. Thermo-viscoelastic model validation from 100% to 300% strains at 0.1/s strain rate: (a) 0 °C, (b) 80 °C.

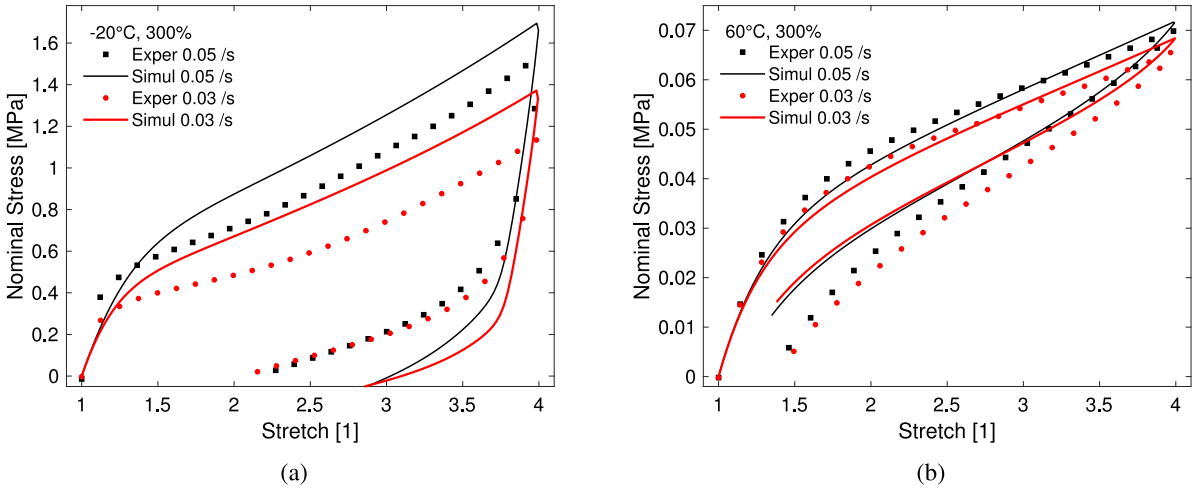

Fig. 19. Thermo-viscoelastic model validation from 0.03/s to 0.05/s strain rates of 300% strain: (a) −20 °C, (b) 60 °C.

are not exactly the same between the simulation and experimental data, these show the same curve tendency and the same strain dependence. We also validate the strain rate dependence at different temperatures, i.e., −20 °C and 60 °C. Fig. 19 shows that both strain rates can be predicted quite well although stress values between two tests differ by more than 20 times. In summary, our model matches the experimental data quite well with a satisfactory agreement.

5. Conclusion

In this contribution, a detailed thermo-viscoelastic experimental characterization of the widely-used VHB polymer is presented. In order to quantify viscoelastic behaviour of the polymer, all classical experimentations, i.e., quasi-static tests at very low strain rates, single-step and multi-step relaxation tests, and loading–unloading cyclic tests are conducted at different strain rates and at different temperatures. Relevant viscoelastic experiments reveal a pronounced influence of the temperature on the VHB polymer where an increasing positive temperature above the reference temperature (room temperature) softens the material mechanically and vice-versa. A thermodynamically consistent phenomenologically motivated thermo-viscoelastic material model at finite strain is proposed where the time-invariant hyperelastic part is derived from a Carrol type energy function. At first, we identify hyperelastic material parameters of the Carrol type model using the quasi-static experimental data. For viscoelastic parameter identification, a simultaneous optimization technique is used taking three different strain rate data at room temperature into account, which helps in finding the best sets of material parameters. Once a complete set of viscoelastic parameters is identified, we use them to validate other sets of data that are not utilized in any identification process. All validation examples show a satisfactory agreement between model and experimental data. Since VHB is extensively used as a dielectric elastomer, in a forthcoming contribution, thermo-electro-viscoelastic experimentation will be presented and data will be compared with a thermo-electro-mechanically coupled computational model.

Acknowledgements

The first two authors would like to extend their sincere appreciation to Zienkiewicz Centre for Computational Engineering (ZCCE), Swansea University, UK for supporting the work. This support facilitates an exchange visit of the first author to ZCCE. The second, fourth and fifth authors acknowledge the funding by DFG, Germany within project STE 544/52-2.

References

[1] A. Ask, A. Menzel, M. Ristinma, Phenomenological modeling of viscous electrostrictive polymers, Int. J. Non-Linear Mech. 47 (2) (2012) 156–165.
[2] D.K. Vu, P. Steinmann, G. Possart, Numerical modeling of non-linear electroelasticity, Internat. J. Numer. Methods Engrg. 70 (2007) 685–704.
[3] D.K. Vu, P. Steinmann, A 2-d coupled BEM-fem simulation of electro-elastostatics at large strain, Comput. Methods Appl. Mech. Engrg. 199 (2010) 1124–1133.
[4] J.P. Pelteret, D. Davydov, A. McBride, D.K. Vu, P. Steinmann, Computational electro-elasticity and magneto-elasticity for quasi-incompressible media immersed in free space, Internat. J. Numer. Methods Engrg. 108 (11) (2016) 1307–1342.
[5] B.A. Alshammari, F. Al-Mubaddel, M.R. Karim, M. Hossain, A.M. Al-Mutairi, A.N. Wilkinson, Addition of graphite filler to enhance electrical, morphological, thermal, and mechanical properties in poly (ethylene terephthalate): Experimental characterization and material modeling, Polymers 11 (9) (2019) 1411.
[6] Z.M. Dang, J.K. Yuan, J.W. Zha, T. Zhou, S.T. Li, G.H. Hu, Fundamentals, Processes and applications of high-permittivity polymer-matrix composites, Prog. Mater. Sci. 57 (4) (2012) 660–723.
[7] C. Ellingford, C. Bowen, T. McNally, C. Wan, Intrinsically tuning the electromechanical properties of elastomeric dielectrics: A chemistry perspective, Macromol. Rapid Commun. 39 (18) (2018) 1800340.
[8] M.A. Keip, P. Steinmann, J. Schroeder, Two-scale computational homogenization of electro-elasticity at finite strains, Comput. Methods Appl. Mech. Engrg. 278 (2014) 62–79.
[9] M. Hossain, Modelling the curing process with a dispersion-type anisotropy in particle-filled electro-active polymers, Contin. Mech. Thermodyn. (2019) http://dx.doi.org/10.1007/s00161-019-00747-5.
[10] M. Wissler, E. Mazza, Mechanical behaviour of an acrylic elastomer used in dielectric elastomer actuators, Sensors Actuators A 134 (2007) 494–504.
[11] M. Hossain, Modelling and Computation of Polymer Curing (PhD Dissertation), University of Erlangen–Nuremberg, Germany, 2010.
[12] M. Mehnert, P. Steinmann, On the influence of the compliant electrodes on the mechanical behavior of VHB 4905, Comput. Mater. Sci. 160 (1) (2019) 287–294.
[13] M. Hossain, D.K. Vu, P. Steinmann, Experimental study and numerical modelling of VHB 4910 polymer, Comput. Mater. Sci. 59 (2012) 65–74.
[14] K. Patra, R.K. Sahu, A visco-hyperelastic approach to modelling rate-dependent large deformation of a dielectric acrylic elastomer, Int. J. Mech. Mater. Des. 11 (1) (2015) 79–90.
[15] R. Sahu, K. Patra, J. Szpunar, Experimental study and numerical modelling of creep and stress relaxation of dielectric elastomers, Strain 51 (1) (2015) 43–54.
[16] M. Mehnert, M. Hossain, P. Steinmann, On nonlinear thermo-electro-elasticity, Proc. R. Soc. A 472 (2016).
[17] D. Ahmad, K. Patra, Experimental and theoretical analysis of laterally pre-stretched pure shear deformation of dielectric elastomer, Polym. Test. 75 (2019) 291–297.
[18] D. Ahmad, M. Hossain, K. Patra, Experimental study and phenomenological modelling of flaw sensitivity of two polymers used as dielectric elastomers, https://doi.org/10.1007/s00161-019-00817-8 (2019).
[19] J. Guo, R. Xiao, H.S. Park, T.D. Nguyen, The temperature-dependent viscoelastic behavior of dielectric elastomers, J. Appl. Mech. 82 (091009) (2015) 1–9.
[20] A. Lion, A physically based method to represent the thermo-mechanical behaviour of elastomers, Acta Mech. 123 (1997) 1–25.
[21] G. Holzapfel, J. Simo, A new viscoelastic constitutive model for continuous media at finite thermodynamical changes, Int. J. Solids Struct. 33 (1996) 3019–3034.
[22] G.A. Holzapfel, Nonlinear Solid Mechanics: A Continuum Approach for Engineering, Wiley & Sons Ltd, UK, 2000.
[23] J.C. Simo, On a full three dimensional finite strain viscoelastic damage model: formulation and computational aspects, Comput. Methods Appl. Mech. Engrg. 60 (1987) 153–173.
[24] M. Kaliske, H. Rothert, Formulation and implementation of three-dimensional viscoelasticity at small and finite strains, Comput. Mech. 19 (1997) 228–239.
[25] J.S. Bergström, M.C. Boyce, Constitutive modeling of the large strain time-dependent behaviour of elastomers, J. Mech. Phys. Solids 46 (1998) 931–954.
[26] J.S. Bergström, Large Strain Time-Dependent Behaviour of Elastomeric Materials (PhD Dissertation), MIT, USA, 1999.
[27] C. Miehe, S. Göktepe, F. Lulei, A micro-macro approach to rubber-like materials: Part-I, the non-affine micro-sphere model of rubber elasticity, J. Mech. Phys. Solids 52 (2004) 2617–2660.
[28] C. Miehe, S. Göktepe, A micro-macro approach to rubber-like materials: Part-II, the micro-sphere model of finite rubber viscoelasticity, J. Mech. Phys. Solids 53 (2005) 2231–2258.
[29] H. Dal, M. Kaliske, Bergström-Boyce model for nonlinear finite rubber viscoelasticity: Theoretical aspects and algorithmic treatment for the FE method, Comput. Mech. 44 (2009) 809–823.
[30] Y. Xiang, D. Zhong, P. Wang, T. Yin, H. Zhou, H. Yu, C. Baliga, S. Qu, W. Yang, A physically based visco-hyperelastic constitutive model for soft materials, J. Mech. Phys. Solids (2019) http://dx.doi.org/10.1016/j.jmps.2019.04.010.
[31] P. Saxena, M. Hossain, P. P. Steinmann, A theory of finite deformation magneto-viscoelasticity, Int. J. Solids Struct. 50 (24) (2013) 3886–3897.
[32] N. Huber, C. Tsakmakis, Finite deformation viscoelasticity laws, Mech. Mater. 32 (2000) 1–18.
[33] S. Reese, S. Govindjee, A theory of finite viscoelasticity and numerical aspects, Int. J. Solids Struct. 35 (1998) 3455–3482.
[34] S. Reese, S. Govindjee, Theoretical and numerical aspects in the thermo-viscoelastic material behaviour of rubber-like polymers, Mech. Time-Depend. Mater. 1 (4) (1997) 357–396.
[35] A.F.M.S. Amin, A. Lion, S. Sekita, Y. Okui, Nonlinear dependence of viscosity in modeling the rate-dependent response of natural and high damping rubbers in compression and shear: Experimental identification and numerical verification, Int. J. Plast. 22 (2006) 1610–1667.
[36] A.F.M.S. Amin, M.S. Alam, Y. Okui, An improved hyperelasticity relation in modeling viscoelasticity response of natural and high damping rubbers in compression: Experiments, parameter identification and numerical verification, Mech. Mater. 34 (2002) 75–95.
[37] N. Koprowski, M. Johlitz, S. Diebels, Characterizing the time dependence of filled EPDM, Rubber Chem. Technol. 84 (2) (2011) 147–165.
[38] N. Koprowski, M. Johlitz, S. Diebels, Modelling of a cellular rubber with non-linear viscosity functions, Exp. Mech. 51 (2011) 749–765.
[39] M. Johlitz, H. Steeb, S. Diebels, A. Chatzouridou, J. Batal, W. Possart, Experimental and theoretical investigation of nonlinear viscoelastic polyurethane systems, J. Mater. Sci. 42 (2007) 9894–9904.
[40] M. Johlitz, D. Scharding, S. Diebels, J. Retka, A. Lion, Modelling of thermo-viscoelastic material behaviour of polyurethane close to the glass transition temperature, Z. Angew. Math. Mech. (ZAMM) 90 (5) (2010) 387–398.
[41] C. Masri, G. Chagnon, D. Favier, H. Sartelet, E. Girard, Experimental characterization and constitutive modeling of the biomechanical behavior of male human urethral tissues validated by histological observations, Biomechanics and modeling in mechanobiology 17 (4) (2018) 939–950.
[42] M. Rebouah, G. Chagnon, Extension of classical viscoelastic models in large deformation to anisotropy and stress softening, Int. J. Non-Linear Mech. 61 (2014) 54–64.
[43] K. Haldar, C. Pal, Rate dependent anisotropic constitutive modeling of brain tissue undergoing large deformation, J. Mech. Behav. Biomed. Mater. 81 (2018) 178–194.

[44] Z.X. Liao, H. Yao, L. Zhang, M. Hossain, J. Wang, S. Zang, Temperature and strain rate dependent large tensile deformation and tensile failure behavior of transparent polyurethane at intermediate strain rates, Int. J. Impact Eng. 129 (2019) 152–167.
[45] L.W. Morland, E.H. Lee, Stress analysis for linear viscoelastic materials with temperature variation, Trans. Soc. Rheol. 4 (1960) 233–263.
[46] R. Muki, E. Sternberg, On transient thermal stresses in viscoelastic materials with temperature-dependent properties, J. Appl. Mech. 28 (1961) 193–207.
[47] K. Sedlan, Viscoelastisches Materialverhalten Von Elastomerwerkstoffen, Experimentelle Untersuchung and Modellbildung (in German) (PhD Dissertation), Universität Kassel, Germany, 2001.
[48] R. Behnke, M. Kaliske, M. Klueppel, Thermo-mechanical analysis of cyclically loaded particle-reinforced elastomer components: experiment and finite element simulation, Rubber Chem. Technol. 89 (1) (2016) 154–176.
[49] B. Dippel, M. Johlitz, A. Lion, Thermo-mechanical couplings in elastomers-experiments and modelling, Z. Angew. Math. Mech. (ZAMM) 95 (11) (2015) 1117–1128.
[50] T. Scheffer, F. Goldschmidt, S. Diebels, Implementation of the strongly pronounced non-linear viscoelasticity of an incompressible filled rubber, Tech. Mech. 35 (2) (2015) 118–132.
[51] H. Seibert, T. Scheffer, S. Diebels, Thermomechanical characterisation of cellular rubber, Contin. Mech. Thermodyn. 28 (5) (2016) 1495–1509.
[52] M. Mehnert, M. Hossain, P. Steinmann, Numerical modeling of thermo-electro-viscoelasticity with field-dependent material parameters, Int. J. Non-Linear Mech. 126 (2018) 13–25.
[53] J. Lubliner, A model of rubber viscoelasticity, Mech. Res. Commun. 12 (2) (1985) 93–99.
[54] C. Linder, M. Tkachuk, C. Miehe, A micromechanically motivated diffusion-based transient network model and its incorporation into finite rubber viscoelasticity, J. Mech. Phys. Solids 59 (2011) 2134–2156.
[55] F. Fan, J. Szpunar, Characterization of viscoelasticity and self-healing ability of VHB 4910, Macromol. Mater. Eng. 300 (1) (2014) 99–106.
[56] S. Lu, K. Pister, Decomposition of deformation and representation of the free energy function for isotropic thermoelastic solids, Int. J. Solids Struct. 11 (7–8) (1975) 927–934.
[57] P. Erbts, A. Duester, Accelerated staggered coupling schemes for problems of thermoelasticity at finite strains, Comput. Math. Appl. 64 (8) (2012) 2408–2430.
[58] L.R.G. Treloar, The Physics of Rubber Elasticity, Oxford University Press, USA, 1975.
[59] J. Nowinski, B. Boley, Theory of thermoelasticity with applications, J. Appl. Mech. 47 (1980) 459.
[60] M.M. Carroll, A strain energy function for vulcanized rubbers, J. Elasticity 103 (2011) 173–187.
[61] P. Steinmann, M. Hossain, G. Possart, Hyperelastic models for rubber-like materials: Consistent tangent operators and suitability of treloar's data, Arch. Appl. Mech. 82 (9) (2012) 1183–1217.
[62] M. Hossain, P. Steinmann, More hyperelastic models for rubber-like materials: Consistent tangent operator and comparative study, J. Mech. Behav. Mater. 22 (1–2) (2013) 27–50.
[63] M. Hossain, N. Kabir, A.F.M.S. Amin, Eight-chain and full-network models and their modified versions for rubber hyperelasticity : A comparative study, J. Mech. Behav. Mater. 24 (1–2) (2015) 11–24.